Absorbing-Boundary Conditions Using Perfectly Matched-Layer (PML) Technique for Three-Dimensional TLM Simulations

Nestor Peña and Michel M. Ney, *Senior Member, IEEE*

***Abstract*— This paper describes the algorithm that interfaces the three-dimensional (3-D) transmission-line matrix (TLM) with an absorbing-boundary condition (ABC) based on the perfectly matched-layer (PML) approach. The algorithm uses a coupling between the TLM symmetrical condensed node (SCN) network and a finite-difference approximation of the PML equations. Examples are presented in scattering problems and S-parameter characterization of discontinuities. Excellent results are found even with absorbing walls located in the region of evanescent waves. Absorption performance obtained are significantly superior to ABC's based on the *one-way equation* approach and currently used for TLM simulations. Finally, it is found that for all tested situations, the algorithm is numerically stable.**

I. Introduction

THE USE OF numerical methods such as transmission-line-matrix symmetrical condensed node (TLM–SCN) [1] or the finite-difference time-domain (FDTD) method [2] requires absorbing conditions at the limit of the computational domain. These conditions have to simulate open space for scattering problems or matched load in the case of guide discontinuity problems, over a wide frequency range and arbitrary wave incidence. Several authors have proposed the absorbing-boundary condition (ABC) algorithm for TLM simulations. A pioneering work used Taylor's series extrapolation and compared it with Higdon's ABC [3]. Other approaches used stability factors to eliminate instabilities produced by Higdon's conditions [4]. More recently, super-absorbing conditions [5] and the Johns matrix technique [6] were presented for guided-wave problems. It is now generally recognized that the perfectly matched-layer (PML) technique originally proposed by Bérenger for FDTD field computations in open space [7], [9] has performances that are significantly superior to other techniques based on the *one-way equation* approach [3]–[5], [10]. However, the algorithm used for the standard Yee's scheme used in the FDTD method cannot be transposed to the SCN–TLM algorithm in a straightforward manner. Indeed, on a boundary which limits the TLM network, all voltages reflected from the absorbing wall are required in order to continue the iterative process. On the other hand, the FDTD method requires the tangential components of either the electric or magnetic field on the absorbing boundary. In spite of this apparent difference, the problem remains of the same nature, as incident and reflected voltages at TLM arms are linear combinations of electric and magnetic fields, which are tangential at the cell faces [11]. Hence, based on this equivalence, this paper presents the algorithm that interfaces a TLM computational domain with a PML domain, in which a finite-difference form of the governing equations is applied.

Theoretically, the PML technique is very attractive, as excellent absorbing performances can be obtained over a wide frequency range and at an arbitrary angle of incidence. More importantly, the computational domain can be significantly reduced as PML boundaries can be located relatively near scatterers or discontinuities [12]. This demonstrates the ability of this absorbing conditions to handle evanescent waves or modes. Concerning the implementation of PML–TLM techniques, two different approaches can be considered: coupling of the TLM network with a FDTD–PML algorithm at the interface [8] (nonunified algorithm) or implementation of a TLM node valid in a PML region [9] (unified algorithm). There is a potential advantage of the nonunified algorithm in terms of computer-memory requirement: only 12 field components (including PML subterms) have to be manipulated, whereas at least 24 variables would be necessary for the SCN–TLM. However, as the three-dimensional (3-D) SCN–TLM and the FDTD Yee's algorithms are not equivalent [13] in terms of numerical dispersion characteristics, parasitic reflections can be expected to occur at the TLM–FDTD PML interface. Concerning this issue, recent work by Eswarappa and Hoefer [14] (in which a coupling between the 3-D TLM and FDTD method in homogeneous space is presented) tends to confirm that excellent matching can be achieved. Keeping in mind the potential gain in computer cost, the nonunified algorithm alternative is chosen for implementation of the PML technique, although this medium has characteristics which are completely different from homogeneous physical media. This constitutes the challenging aspect of this paper.

II. Theory

The TLM numerically models electromagnetic-field time evolution at the center of a cell from incident $\vec{a}$ and reflected $\vec{b}$ voltages at all ports of the node shown in Fig. 1(a). Thus, if at time $(n-1/2)\Delta t$ incident voltages are known in the whole TLM network, reflected voltages at time $(n+1/2)\Delta t$ can be computed via a scattering matrix $[S]$, which characterizes the

Manuscript received May 14, 1997; revised June 20, 1997. This work was supported in part by the French Ministère des Affaires Etrangères and by the Colombian Agency Colciencias.

The authors are with the Laboratory for Electronics and Communication Systems (LEST), Ecole Nationale Supèrieure des Tèlècommunications, 29285 Brest Cedex, France.

Publisher Item Identifier S 0018-9480(97)07110-X.

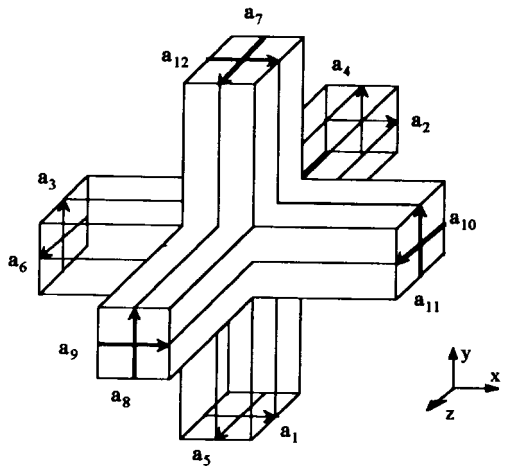

(a)

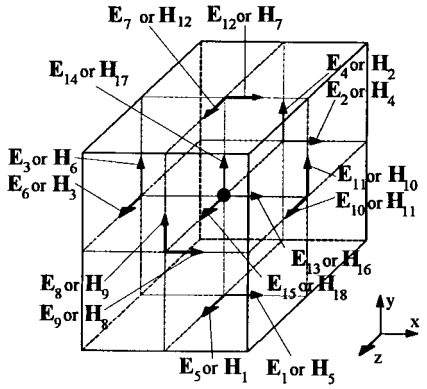

(b)

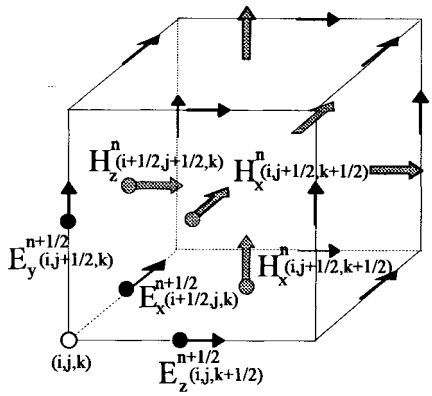

(c)

Fig. 1. Location of field components and voltages in cells. (a) 12 incident voltages of the basic unloaded TLM–SCN (reflected voltages are numbered and polarized the same way). (b) TLM–SCN elementary cell with electric field samples. (c) FDTD Yee's cell.

node [11]

$$\vec{b}^{(n+1/2)\Delta t} = [S]\vec{a}^{(n-1/2)\Delta t}. \tag{1}$$

At the same time, the reflected voltages are transferred to the neighboring nodes to become, in turn, the incident voltages for the next time iteration. If instead of a node, reflected voltages hit a boundary, appropriate conditions must be enforced to determine incident voltages from that boundary which should be entering the node for the next time iteration. For instance, electric or magnetic walls return reflected voltages with reflection coefficient -1 or $+1$, respectively. In fact, field boundary conditions are applied since the total tangential-field components, which corresponds to the linear combination of incident and reflected voltages at the input arm, must vanish in these two cases. Finally, the six field component values at the center of the cell at time $n\Delta t$ are computed from incident voltages (see Fig. 1) as follows:

$$\begin{aligned}
\Delta l \cdot E_x^n &= \tfrac{1}{2}\,(a_1 + a_2 + a_9 + a_{12})^{n-1/2} \\
\Delta l \cdot E_y^n &= \tfrac{1}{2}\,(a_3 + a_4 + a_8 + a_{11})^{n-1/2} \\
\Delta l \cdot E_z^n &= \tfrac{1}{2}\,(a_5 + a_6 + a_7 + a_{10})^{n-1/2} \\
Z_0 \Delta l \cdot H_x^n &= \tfrac{1}{2}\,(-a_4 + a_5 - a_7 + a_8)^{n-1/2} \\
Z_0 \Delta l \cdot H_y^n &= \tfrac{1}{2}\,(a_2 - a_6 - a_9 + a_{10})^{n-1/2} \\
Z_0 \Delta l \cdot H_z^n &= \tfrac{1}{2}\,(-a_1 + a_3 - a_{11} + a_{12})^{n-1/2}
\end{aligned} \tag{2}$$

in the case of a cubic SCN cell ($\Delta l = \Delta_x = \Delta_y = \Delta_z$) and where Z_0 is the free-space intrinsic impedance. Note that for rectangular cells, stub loading must be used, and the above expressions become more complex [11]. Nevertheless, the proposed algorithm remains the same for rectangular cells.

One important feature of the TLM using the SCN (including the hybrid symmetrical condensed node (HSCN) [15] and symmetrical supercondensed node (SSCN) [16]) is the nature of the voltages $\vec{a}$ and $\vec{b}$. They are linear combinations of field components tangential to the cell at the arm access, as illustrated by Fig. 1(b), in which voltage numbering originally used by Johns is utilized [1]. For instance, voltages a_9 and b_9 are given by

$$\begin{Bmatrix} a_9 \\ b_9 \end{Bmatrix} = \tfrac{1}{2}\,(\Delta_x E_9^x \mp Z_9 \Delta_y H_9^y) \tag{3}$$

where Z_9 is related to the characteristic impedance of the arm in which voltages propagate, and its value depends on the type of SCN node [11]. Hence, if at time $(n+1/2)\Delta t$, b_9 and E_9^x (or H_9^y) are known, one can uniquely determine from (3) the incident voltage a_9 for the next iteration. The algorithm to couple the TLM and FDTD–PML network is inspired from the above relation.

First of all, let us consider the PML region and the governing equations which amount to 12 in the 3-D case. Each field component is separated into two terms whose time evolution is related to spatial variations of other dual field components. For instance, the time variation of $E_x = E_{xy} + E_{xz}$ in the PML region becomes [7]

$$\begin{aligned}
\varepsilon_0 \frac{\partial E_{xy}}{\partial t} + \sigma_y E_{xy} &= \frac{\partial (H_{zx} + H_{zy})}{\partial y} = \frac{\partial H_z}{\partial y} \\
\varepsilon_0 \frac{\partial E_{xz}}{\partial t} + \sigma_z E_{xz} &= -\frac{\partial (H_{yz} + H_{yx})}{\partial z} = -\frac{\partial H_y}{\partial z}
\end{aligned} \tag{4}$$

in which (σ_i, σ_i^*) where $i \in \{x, y, z\}$ are electric and magnetic conductivities, respectively, satisfying the following condition [7]:

$$\frac{\sigma_i}{\varepsilon_0} = \frac{\sigma_i^*}{\mu_0}. \tag{5}$$

The approximation of (4) can be achieved by taking the FD of subterms (for instance, E_{xy} and E_{xz}) at the same location and time as in the standard FDTD Yee's scheme [17] [see Fig. 1(c)]. The usual notation takes the origin of coordinates at the edge of any cell and field samples are written as follows:

$$\begin{aligned}
E_x^n(i,j,k) &= E_x\left[\left(i+\tfrac{1}{2}\right)\Delta_x, j\Delta_y, k\Delta_z, \left(n+\tfrac{1}{2}\right)\Delta t\right]\\
E_y^n(i,j,k) &= E_y\left[i\Delta_x, \left(j+\tfrac{1}{2}\right)\Delta_y, k\Delta_z, \left(n+\tfrac{1}{2}\right)\Delta t\right]\\
E_z^n(i,j,k) &= E_z\left[i\Delta_x, j\Delta_y, \left(k+\tfrac{1}{2}\right)\Delta_z, \left(n+\tfrac{1}{2}\right)\Delta t\right]\\
H_x^n(i,j,k) &= H_x\left[i\Delta_x, \left(j+\tfrac{1}{2}\right)\Delta_y, \left(k+\tfrac{1}{2}\right)\Delta_z, n\Delta t\right]\\
H_y^n(i,j,k) &= H_y\left[\left(i+\tfrac{1}{2}\right)\Delta_x, j\Delta_y, \left(k+\tfrac{1}{2}\right)\Delta_z, n\Delta t\right]\\
H_z^n(i,j,k) &= H_z\left[\left(i+\tfrac{1}{2}\right)\Delta_x, \left(j+\tfrac{1}{2}\right)\Delta_y, k\Delta_z, n\Delta t\right]. \quad (6)
\end{aligned}$$

The next step is to take a different form of (4), using the above notation (6). Then, since one wants to interface the FDTD algorithm with the TLM, one expresses fields in terms of voltages, which for cubic cell (without loss of generality) and setting $\Delta t = \Delta l/2c_0$ are given by

$$V_{ers}^n(i,j,k) = \Delta l \cdot E_{rs}^n(i,j,k), \quad \text{with } (r,s) \in \{(x,y),(x,z)\} \quad (7)$$

$$V_{ms}^n(i,j,k) = \sqrt{\frac{\mu_0}{\varepsilon_0}}\,\Delta l \cdot H_s^n(i,j,k), \qquad \text{with } s \in \{y,z\} \quad (8)$$

where subscripts e and m refer to electric and magnetic, respectively. Finally, after some algebraic manipulations, one obtains the time evolution of field subterms in terms of the following voltages:

$$\begin{aligned}
V_{exy}^n(i,j,k) &= \left(\frac{4-G_{ey}}{4+G_{ey}}\right)V_{exy}^{n-1}(i,j,k)\\
&\quad + \left(\frac{2}{4+G_{ey}}\right)\{V_{mz}^n(i,j,k)\\
&\quad - V_{mz}^n(i,j-1,k)\}\\
V_{exz}^n(i,j,k) &= \left(\frac{4-G_{ez}}{4+G_{ez}}\right)V_{exz}^{n-1}(i,j,k)\\
&\quad - \left(\frac{2}{4+G_{ez}}\right)\{V_{my}^n(i,j,k)\\
&\quad - V_{my}^n(i,j,k-1)\}\\
V_{ex}^n(i,j,k) &= V_{exy}^n(i,j,k) + V_{exz}^n(i,j,k) \quad (9)
\end{aligned}$$

where $G_{es} = \sqrt{(\mu_0/\varepsilon_0)}\Delta l\sigma_s(i,j,k)$ with $s \in \{y,z\}$. Note that unlike the procedure followed in [7] where an exponential approximation was used for the FDTD–PML, an ordinary central-difference scheme is used here [18].

Now, suppose that there exists an interface between TLM and FDTD–PML networks parallel to the plane Oxy at coordinate $z = k\Delta_z$. In order to continue the iteration process in the PML region, it is necessary to know the electric-field tangential components on this interface [Fig. 2(a)]. Therefore, according to (9), one has to determine the magnetic-field tangential components in the plane located at coordinate $z = (k \pm 1/2)\Delta_z$ and the magnetic-field normal components at the plane $z = k\Delta_z$, but with time delay $\Delta t/2$ to remain consistent with Yee's scheme [Fig. 2(b)]. Finally, the reflected impulse from the interface to the adjacent TLM node is computed from (3) in which interpolated tangential electric-field values in the FDTD network are inserted, yielding

$$a_{8,9}^{n+1/2} = \Delta_{y,x}E_{8,9}^{y,x} - b_{8,9}^{n+1/2} \quad (10)$$

as illustrated by Fig. 2(c). The above procedure is applied again for the next time iteration. One can notice that the proposed coupling algorithm strictly enforces the continuity of magnetic- and electric-field tangential components in the plane $z = (k-1/2)\Delta_z$ and $z = k\Delta_z$, respectively. Also, linear spatial variation is assumed for field-component interpolation. Note that the above procedure is general as the subterms are not directly involved, and it also straightforwardly applied to the basic coupling TLM–FDTD as presented in [14]. However, the proposed coupling algorithm is different from the one presented in [14] in two aspects: the present algorithm involves a region which extends over half a cell (minimum) instead of two cells and the new incident voltage vector is computed by field continuity conditions at the interface instead of at the cell center. However, one cannot evaluate the impact of these differences as this paper is devoted to implementing PML with TLM computations rather than interfacing the TLM and FDTD method.

III. Results

The first step to evaluate the reflection performance of the proposed algorithm is to consider the empty WR-28 rectangular waveguide ($a = 7.112$ mm $= 36\Delta l$) illustrated in Fig. 3, which is terminated at both ends with a PML region. The dominant mode TE_{10} is generated by a current sheet [11], with amplitude-modulated Gaussian-pulse time variation (central frequency: 32.5 GHz, 15 GHz bandwidth), located near one PML boundary. The reflection coefficient was computed with reference to an infinitely long waveguide. A parabolic profile ($\sigma_{\max} = 25$ S/m) was used for the PML regions and comparison with a full-FDTD (uniform FDTD algorithm) simulation under the same conditions is also shown in Fig. 3. If the TLM FDTD–PML algorithm yields excellent performance with reflection level below -55 dB over the full operating range, much better performance is still obtained with the full FDTD algorithm. This difference can be explained by the nonuniform nature of the proposed algorithm, as the different dispersion behavior between TLM and FDTD networks may play a significant role [12]. The source of local reflections may also be triggered by interpolation processes at the interface between TLM and FDTD–PML networks. However, the reflection level is much below the one obtained by other ABC's applied to TLM computations [3].

The next step is to evaluate the reflection performance when evanescent modes are present near the TLM-PML interface for a true 3-D problem. Consider the capacitive iris in a WR-28 rectangular waveguide, as illustrated in Fig. 4. It is proposed to compute the S_{11}-parameter over the whole operating range of the guide by exciting the structure under the same conditions (as with the previous example). The TLM–PML interface is purposely located in the region where evanescent modes TE_{1n} and TM_{1n} ($n \neq 0$) are no longer negligible. However, in order to directly extract S_{11} without special treatment for retrieving

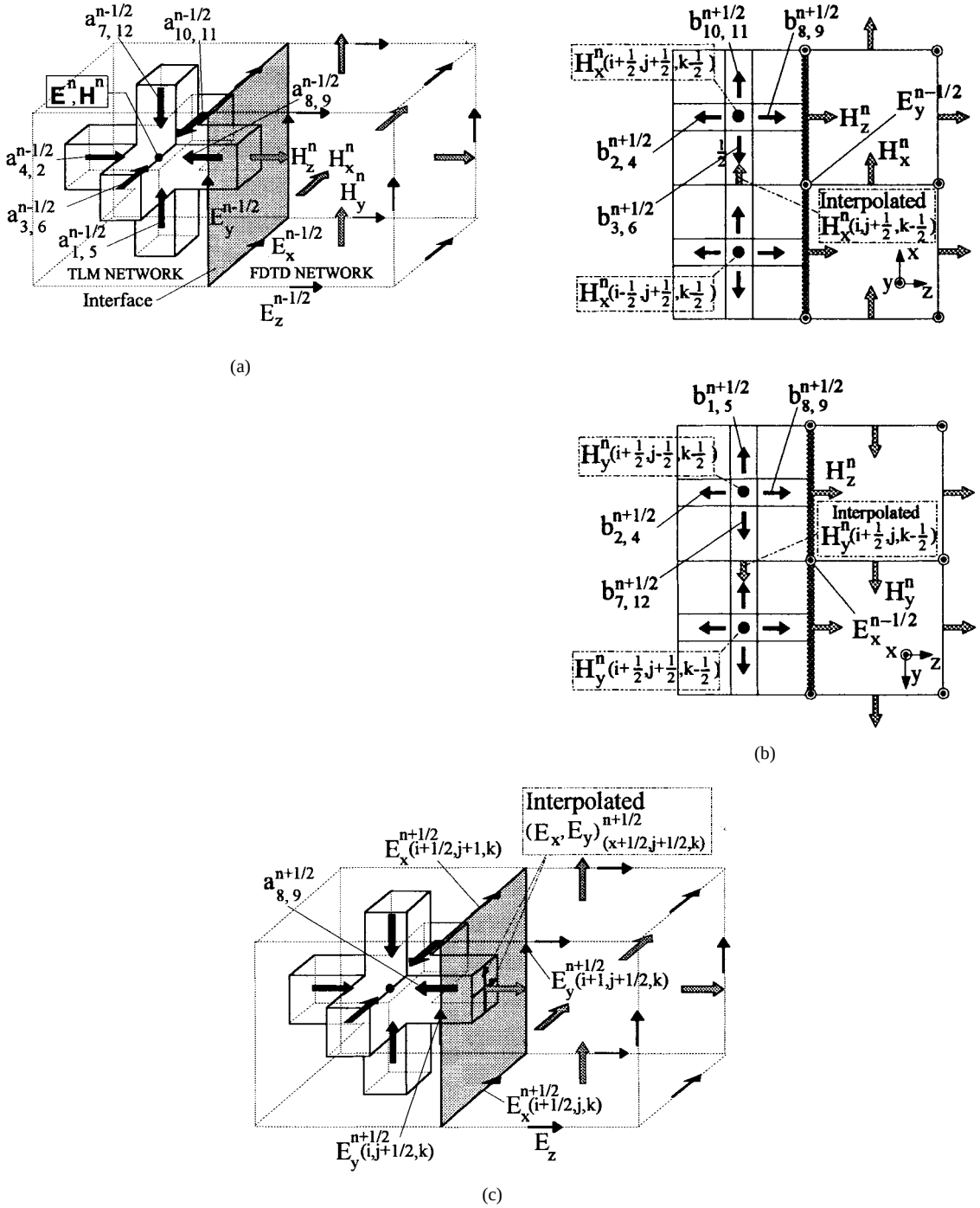

Fig. 2. Illustration of the various steps of the algorithm. (a) *Phase I*: In the TLM network, the total field E^n, H^n at the center of the cell, are computed from the incident waves $a_m^{n-1/2}$ by (2). In the FDTD network, the H^n-field components are computed with the standard algorithm. (b) *Phase II*: Reflected voltages are computed via the standard TLM algorithm. H^n-components required by the FDTD network to compute $E^{n+1/2}$ on the interface are interpolated between two adjacent TLM cells. (c) *Phase III*: Tangential E-components required by the TLM are interpolated from the FDTD values at the cell edges on the interface. TLM impulses are then transferred, except at arms normal to the interface where they are computed from (10). The procedure is now ready for Phase I of the next time-step.

the dominant mode [6], the PML and the excitation on the left are located sufficiently remote from the iris. Finally, in order to minimize coarseness error, results from two simulations with decreasing cell size $\Delta l = a/36$ and $\Delta l = a/66$ (Fig. 4), respectively, were first performed. Linear extrapolation for $\Delta l \to 0$ was then applied. Fig. 5 shows the S_{11}-coefficient magnitude and phase, respectively, in which results obtained by a full FDTD simulation and the Marcuvitz equivalent-circuit formula [19] are included for comparison. Corrections were made to obtain an identical reference plane for all cases. One can notice the excellent agreement between the various approaches and also the slightly better convergence for the full-FDTD algorithm as the step size Δl is reduced. However, extrapolated values are almost identical in both

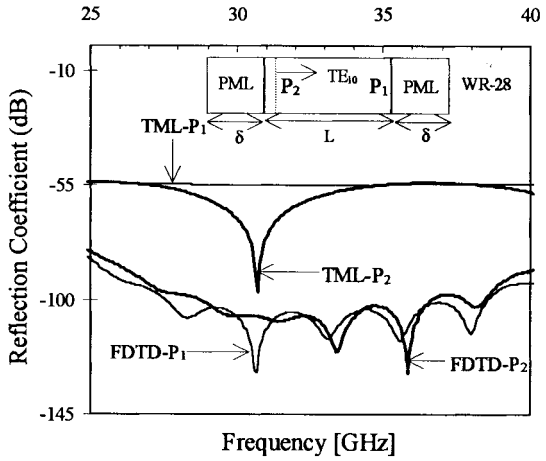

Fig. 3. ABC's reflection performance and geometry for the case of an empty WR-28 waveguide ($L = 60\Delta l$ and $\delta = 25\Delta l$, $\sigma_{\max} = 25$ S/m).

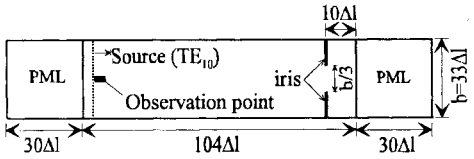

Fig. 4. Geometry for capacitive iris S_{11}-parameter computation ($\Delta l = a/66$, $\sigma_{\max} = 50$ S/m).

cases. The discrepancy with the FDTD can be explained by the presence of metallic edges for which the TLM produces coarseness error superior to the FDTD. This peculiarity, which is not addressed in this paper, was investigated by several authors [6], [20], and solutions to overcome the problem were proposed. However, as the mesh size is reduced, discrepancies between both methods tend to vanish. Finally, one can notice the good performance of the PML located near discontinuities where nonnegligible evanescent modes prevail (mostly the TM_{11} in this case). Fig. 6 clearly shows that at the PML interface location, evanescent modes are not negligible and are unperturbed by the presence of the PML as compared to the benchmark solution. It is worth mentioning that yet unperturbed evanescent waves do not experience additional attenuation from the PML medium. Thus, one has to make sure that the layer thickness is sufficiently large, especially when one gets near cutoff. This issue is addressed in a paper by Fang *et al.* [21].

The proposed algorithm is applied to the scattering of a perfectly conducting cube (Fig. 7) and compared with a field integral equation solved by the method of moments (MoM) for which no ABC is required. This problem was also investigated with the FDTD method using the second-order Mur's ABC [22], as well as with the TLM using Higdon's and Taylor's ABC [3]. For the FDTD method, the cube of normalized size k_0a was sampled by 20^3 cells and the ABC located at $15\Delta l$ ($0.75a$) from the cube. For TLM simulations, the cube was sampled with 12^3 cells and ABC's were located at $15\Delta l$ ($1.25a$) from the cube. Again to confirm the ability of the algorithm to handle evanescent waves, the TLM–PML interface is placed at only $5\Delta l$ ($0.24a$) from the scatterer.

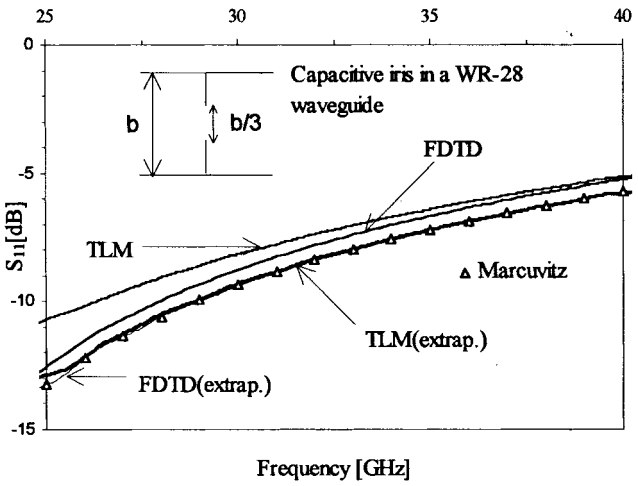

(a)

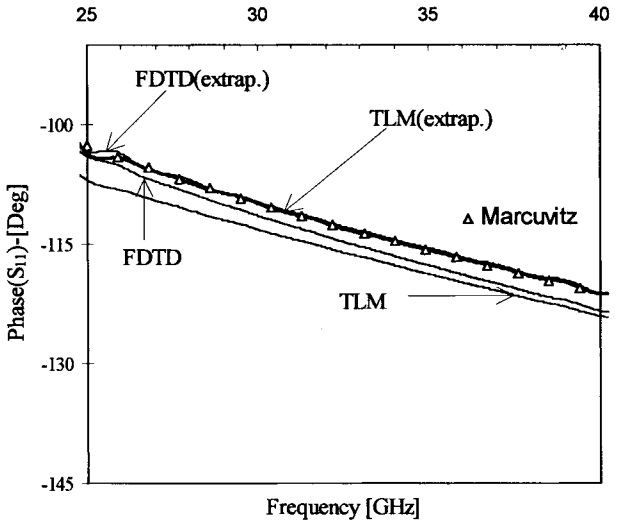

(b)

Fig. 5. Computed S_{11} for the geometry illustrated in Fig. 4 with comparison between different approaches. (a) Magnitude. (b) Phase.

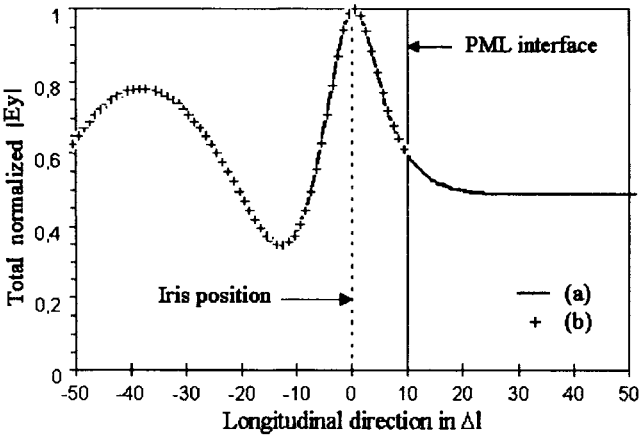

Fig. 6. Longitudinal distribution of the E-field magnitude in the middle of the waveguide in the case illustrated in Fig. 4. Benchmark solution (solid line). With PML interface (crosses).

In all cases, equivalent Huygens surface [3], [22] was used for excitation. For the last case, TLM–PML interfaces were

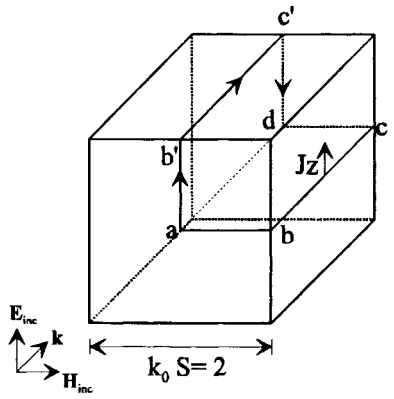

Fig. 7. Geometry for perfectly conducting cube (dimension S) scattering problem.

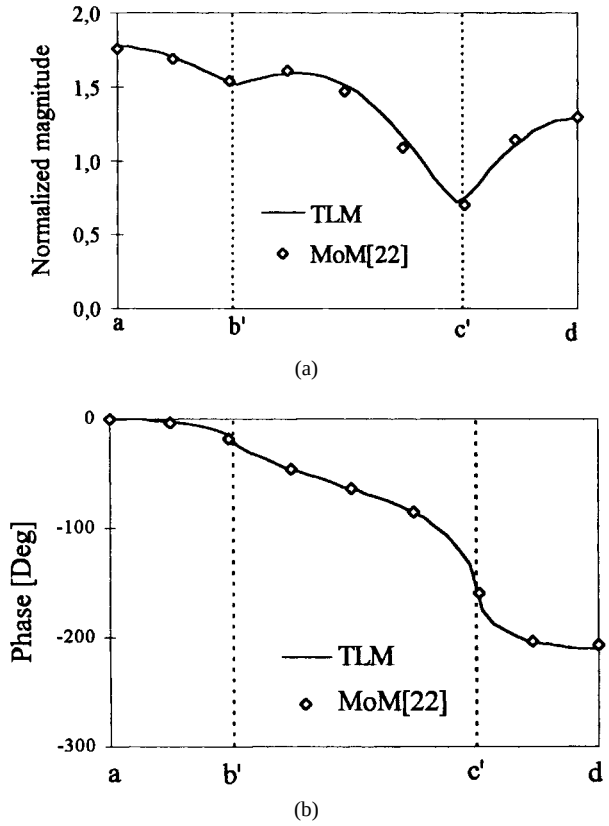

Fig. 8. Current density distribution along path $\overline{\mathrm{ab'c'd}}$. (a) Magnitude normalized to H_{inc} and (b) phase difference relative to point a (see Fig. 7).

located only at $2\Delta l$ from the equivalent source surface. Finally, the PML thickness was 12 cells with a 10^{-5}-reflection factor at normal incidence.

The current density on the cube is determined from the tangential magnetic-field components, and a fast Fourier transform (FFT) is performed to obtain current values at a location over a wide frequency range. Fig. 8 shows the comparison between the proposed algorithm and the MoM (32 triangles per face) [22] for the current density along the path $\overline{\mathrm{ab'c'd}}$ in both magnitude and phase (normalized frequency $k_0\mathrm{S} = 2$). In Fig. 9, the current density component J_z on the lateral side of the cube (path $\overline{\mathrm{abcd}}$) is also shown. Excellent agreement can

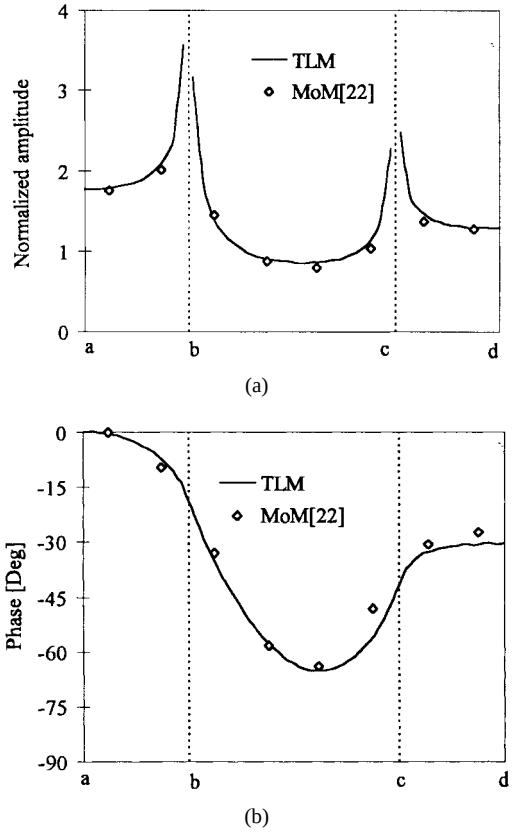

Fig. 9. Current density J_z distribution along the lateral path $\overline{\mathrm{abcd}}$. (a) Magnitude normalized to H_{inc} and (b) phase difference relative to point a (see Fig. 7).

be observed and the TLM perfectly reproduces the singularity which occurs at the cube edges [Fig. 9(a)]. In addition, one may again stress that as compared to other ABC's developed so far for the TLM, a significant gain in computer memory is achieved as PML boundaries are located relatively near the scatterer. Note that results may be improved by optimizing the PML conductivity profile [12]. Finally, no instabilities were observed during long-term simulations.

IV. Conclusions

Bérenger's PML absorbing condition was implemented for 3-D-TLM field computations. A coupling algorithm between the SCN–TLM and the PML region was described. It is based on an FD approximation of the PML equations and a proper interfacing with the TLM algorithm. The so-called nonuniform algorithm involves the junction between networks with different numerical dispersion properties. As a result, performances (although very good) do not reach the level of the full FDTD algorithm. This can be explained by the interpolation which is required at the boundary to couple the TLM and the FDTD–PML algorithms and the difference in the numerical dispersion of both networks. However, the level of reflections is significantly below the one obtained with the published ABC for the TLM so far. Simulation results have shown that the proposed algorithm yields excellent performances for both guiding and open structures. In addition, the ABC can be placed relatively close to discontinuities or

scatterers where evanescent modes or waves prevail without noticeable degradation of performances. Finally, long-duration simulations have shown that the algorithm is stable in all tested situations.

REFERENCES

[1] P. B. Johns, "A symmetrical condensed node for the TLM method," *IEEE Trans. Microwave Theory Tech.*, vol. MTT-35, pp. 370–377, Apr. 1987.

[2] K. S. Yee, "Numerical solution of initial boundary—Value problems involving Maxwell's equations in isotropic media," *IEEE Trans. Antennas Propagat.*, vol. AP-14, pp. 302–307, May 1966.

[3] Z. Chen, M. M. Ney, and W. J. R. Hoefer, "Absorbing and connecting boundary conditions for the TLM method," *IEEE Trans. Microwave Theory Tech.*, vol. 41, pp. 2016–2024, Nov. 1993.

[4] C. Eswarappa and W. J. R. Hoefer, "One-way equation absorbing boundary conditions for 3-D TLM analysis of planar and quasi-planar structures," *IEEE Trans. Microwave Theory Tech.*, vol. 42, pp. 1669–1677, Sept. 1994.

[5] N. Kukutsu and R. Konno, "Super absorption boundary condition for guided waves in the 3-D TLM simulation," *IEEE Microwave Guided Wave Lett.*, vol. 5, pp. 299–301, Sept. 1995.

[6] M. Righi and W. J. R. Hoefer, "Efficient 3-D SCN-TLM diakoptics for waveguide components," *IEEE Trans. Microwave Theory Tech.*, vol. 42, pp. 2381–2385, Dec. 1994.

[7] J. P. Bérenger, "A perfectly matched layer for the absorption of electromagnetic waves," *J. Comput. Phys.*, vol. 114, no. 2, pp. 110–117, Oct. 1994.

[8] C. Eswarappa and W. J. R. Hoefer, "Implementation of Bérenger's absorbing boundary conditions in TLM by interfacing FDTD perfectly matched layers," *Electron. Lett.*, vol. 31, no. 15, pp. 1264–1266, July 1995.

[9] N. Peña and M. M. Ney, "A new TLM node for Bérenger's perfectly matched layer (PML)," *IEEE Microwave Guided Wave Lett.*, vol. 6, pp. 410–412, Nov. 1996.

[10] G. Mur, "Absorbing boundary conditions for the finite difference approximation of the time-domain electromagnetic-field equations," *IEEE Trans. Electromag. Compat.*, vol. EMC-23, pp. 377–382, Nov. 1981.

[11] N. Peña and M. M. Ney, "A general formulation of a three-dimensional TLM condensed node with the modeling of electric and magnetic losses and current sources," in *12th Annu. Rev. Progress Appl. Computational Electromagnetics*, Monterey, CA, Mar. 18–22, 1996, pp. 262–269.

[12] J. P. Bérenger, "Perfectly matched layer for the FDTD solution of wave-structure interaction problems," *IEEE Trans. Antennas Propagat.*, vol. 44, pp. 110–117, Jan. 1996.

[13] M. Krumpholz and P. Russer, "On the dispersion in TLM and FDTD," *IEEE Trans. Microwave Theory Tech.*, vol. 42, pp. 1275–1279, July 1994.

[14] C. Eswarappa and W. J. R. Hoefer, "A hybrid 3-D TLM-FDTD model of microwave fields," in *IEEE MTT-S Dig.*, San Francisco, CA, June 17–21, 1996, pp. 1063–1066.

[15] R. Scaramuzza and A. J. Lowery, "Hybrid symmetrical condensed node for the TLM method," *Electron. Lett.*, vol. 26, no. 23, pp. 1947–1948, Nov. 1990.

[16] V. Trenkic, C. Christopoulos, and T. M. Benson, "Theory of the symmetrical super-condensed node for the TLM method," *IEEE Trans. Microwave Theory Tech.*, vol. 43, pp. 1342–1348, June 1995.

[17] R. W. Ziolkowski, N. K. Madsen, and R. C. Carpentier, "Three-dimensional computer modeling of electromagnetic fields: A global look back lattice truncation scheme," *J. Comput. Phys.*, vol. 50, pp. 360–408, 1983.

[18] J. C. Veihl and R. Mittra, "An efficient implementation of Bérenger's perfectly matched layer (PML) for finite-difference time-domain mesh truncation," *IEEE Microwave Guided Wave Lett.*, vol. 6, pp. 94–96, Feb. 1996.

[19] N. Marcuvitz, *Waveguide Handbook*. Boston, MA: Boston Tech. Publishers, 1964.

[20] L. Cascio, G. Tardioli, T. Rozzi, and W. J. R. Hoefer, "A quasi-static modification of TLM at knife edge and 90° wedge singularities," *IEEE Trans. Microwave Theory Tech.*, vol. 44, pp. 2519–2524, Dec. 1996.

[21] J. Fang and Z. Wu, "Generalized perfectly matched layer for the absorption of propagating and evanescent eaves in lossless and lossy media," *IEEE Trans. Microwave Theory Tech.*, vol. 44, pp. 2216–2222, Dec. 1996.

[22] A. Taflove and K. Umashankar, "Radar cross section of general three-dimensional scatterers," *IEEE Trans. Electromag. Compat.*, vol. EMC-25, pp. 433–440, Nov. 1983.

Nestor Peña received the B.Sc. and M.Sc. degrees in electrical engineering, and the B.Sc. degree in mathematics from the Universidad de los Andes, Bogotá, Colombia, in 1987, 1989, and 1991, respectively. He is currently working toward the Ph.D. degree in telecommunications at the Laboratory for Electronics and Communication Systems (LEST), Ecole Nationale Supérieure des Télécommunications (France Telecom Bretagne), Brest Cedex, France.

From 1987 to 1991, he worked as an Engineer with the Consultoria Colombiana S.A., a consulting company for power systems. From 1991 to 1993, he was with the Department of Electrical Engineering, Universidad de los Andes. His research interests are in applied electromagnetics and numerical modeling.

Michel M. Ney (S'80–M'82–SM'91) received the Engineering Diploma from the Swiss Federal Institute of Technology of Lausanne (EPFL), Switzerland, in 1976, the M.Sc. degree from the University of Manitoba, Winnipeg, Man., Canada in 1978, and the Ph.D. degree from the University of Ottawa, Ottawa, Ont., Canada, in 1983.

After returning to Switzerland, he joined the Laboratoire d'électromagnétisme et d'hyperfréquences of the EPFL as a Research Engineer where he worked on the modeling of microwave and antenna systems. In 1983, he joined the Department of Electrical Engineering, University of Ottawa, as an Assistant Professor. In 1990, he spent his sabbatical leave at the Laboratoire d'électromagnétisme et d'acoustique (LEMA) of the EPFL as an Invited Professor, where he gave lectures and participated in international workshops on electromagnetic-field modeling, and in 1993, he became Full Professor. Since 1993, he has been with the Ecole Nationale Supérieure des Télécommunications (France Telecom Bretagne), Brest Cedex, France. His research interests include millimeter-wave circuits, electromagnetic compatibility and interference (EMC/I) problems, and time- and frequency-domain numerical techniques applied to electromagnetic engineering (imaging, antenna).

Dr. Ney is a member of the Laboratory for Electronics and Communication Systems (LEST), which is a research unit associated with the French National Research Council (CNRS), and a member of the editorial board of the *International Journal of Numerical Modeling: Electronic Networks, Devices and Fields*.